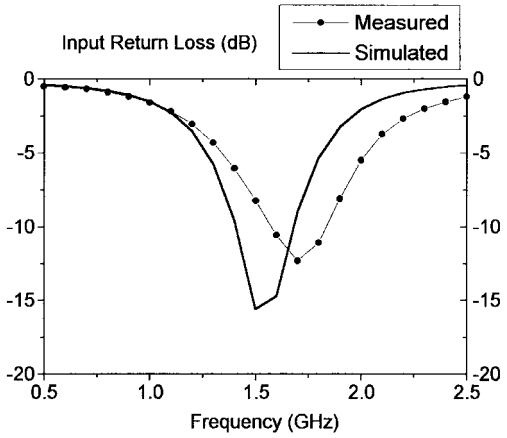

Fig. 6. Plot of measured versus simulated performance of the input return loss (S_{11}) of the fabricated CFLNA.

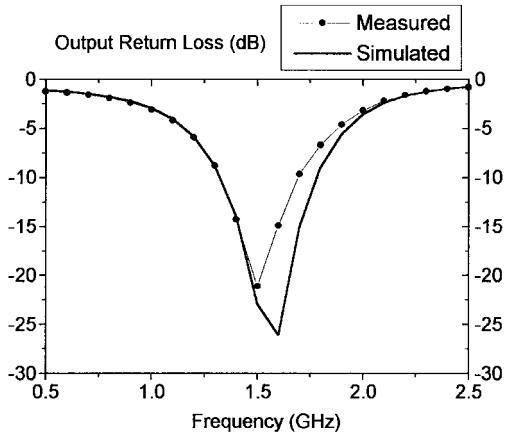

Fig. 7. Plot of measured versus simulated performance of the input return loss (S_{22}) of the fabricated CFLNA.

integrated circuit (MMIC) LNA has been fabricated. The measured response agrees well with the simulated performance. Extensive computer simulation shows that when silicon n-p-n BJT is used, this scheme enables us to make both $\Gamma_{\rm opt}$ and $G_{\rm max}$ points near to 50 Ω, in addition to the simultaneous noise and input power matching.

REFERENCES

[1] R. E. Lehmann and D. D. Heston, "X-band monolithic series feedback LNA," *IEEE Trans. Electron Devices*, vol. ED-32, pp. 2729–2735, Dec. 1985.

[2] J. Engberg, "Simultaneous input power match and noise optimization using feedback," in *Dig. Tech. Paper 4th European Microwave Conf.*, Montreux, Switzerland, Sept. 1974, pp. 385–389.

[3] L. Besser, "Stability consideration of low-noise transistor amplifiers with simultaneous noise and power match," in *IEEE MTT-S Int. Microwave Symp. Dig.*, 1975, pp. 327–329.

[4] K. D. Ross and L. P. Dunleavy, "Simultaneous $NF_{\rm min}$ and $G_{\rm max}$ for LNA Design," in *Proc. EEsof Users Group Meeting*, Atlanta, GA, June 1993.

[5] G. Gonzalez, *Microwave Transistor Amplifiers, Analysis and Design*. Englewood Cliffs, NJ: Prentice-Hall, 1984.

[6] B. K. Ko, "*Circuit Design Techniques of Monolithic Microwave Low Noise Amplifiers*," Ph.D. dissertation, Dept. Elect. Eng., Korea Advanced Institute Sci. Technol., Taejeon, Korea, 1997.

A Large-Signal Characterization of an HEMT Using a Multilayered Neural Network

Kazuo Shirakawa, Masahiko Shimiz, Naofumi Okubo, and Yoshimasa Daido

***Abstract*—We propose an approach to describe the large-signal behavior of a high electron-mobility transistor (HEMT) by using a multilayered neural network. To conveniently implement this in standard circuit simulators, we extracted the HEMT's bias-dependent behavior in terms of conventional small-signal equivalent-circuit elements. We successfully represented seven intrinsic elements with a five-layered neural network (composed of 28 neurons) whose inputs are the gate-to-source bias $(V_{\rm gs})$ and drain-to-source bias $(V_{\rm ds})$. A "well-trained" neural network shows excellent accuracy and generates good extrapolations.**

***Index Terms*—HEMT, large-signal model, neural network.**

I. INTRODUCTION

A large-signal model for an active device, such as a high electron-mobility transistor (HEMT), is an essential tool for accurately designing high-frequency components. Several good models based on closed-form equations [1], [2] and look-up tables [3] have been proposed. Recently, a third approach using a neural network has been reported [4]. The neural-network model is an intermediate approach between the conventional ones, and accurately models a comparatively small database.

However, this reported neural-network model adopts a three-layered configuration which requires numerous neurons.

In this paper, we propose a different multilayered neural-network approach to describe the large-signal behavior of HEMT's. To conveniently implement it on a standard harmonic-balance simulator (such as the HP-MDS), we characterized large-signal behavior with a conventional small-signal equivalent-circuit analysis [5]. The bias-dependent intrinsic elements ($C_{\rm gs}$, R_i, C_{gd}, g_m, τ, $g_{\rm ds}$, and $C_{\rm ds}$) are then described by a neural network whose inputs are $V_{\rm gs}$ and $V_{\rm ds}$. We supplied normalized data for the neural network to obtain a learning convergence and stable extrapolations.

By experimenting, we found that a five-layered network configuration (consisting of only 28 neurons) adequately represents seven intrinsic elements simultaneously. We used a batch-mode back-propagation algorithm [6] and adopted this neural network to several similar devices. The well-trained network displayed excellent accuracy.

II. MULTILAYERED NEURAL NETWORK

Fig. 1 shows a standard multilayered (the number of layers is M) neural network. In this figure, each circle is a neuron, and the boxes enclosing several neurons are the layers. The kth layer includes $(N_k + 1)$ neurons. At the far left is the *input* layer, and at the far right is the *output* layer. The input and output of the ith neuron in

Manuscript received December 29, 1995; revised May 19, 1997.

K. Shirakawa, M. Shimiz, and N. Okubo are with the Fujitsu Laboratories Ltd., Nakahara-ku, Kawasaki, 211 Japan.

Y. Daido is with the Kanazawa Institute of Technology, Ishikawa, 921 Japan.

Publisher Item Identifier S 0018-9480(97)06068-7.

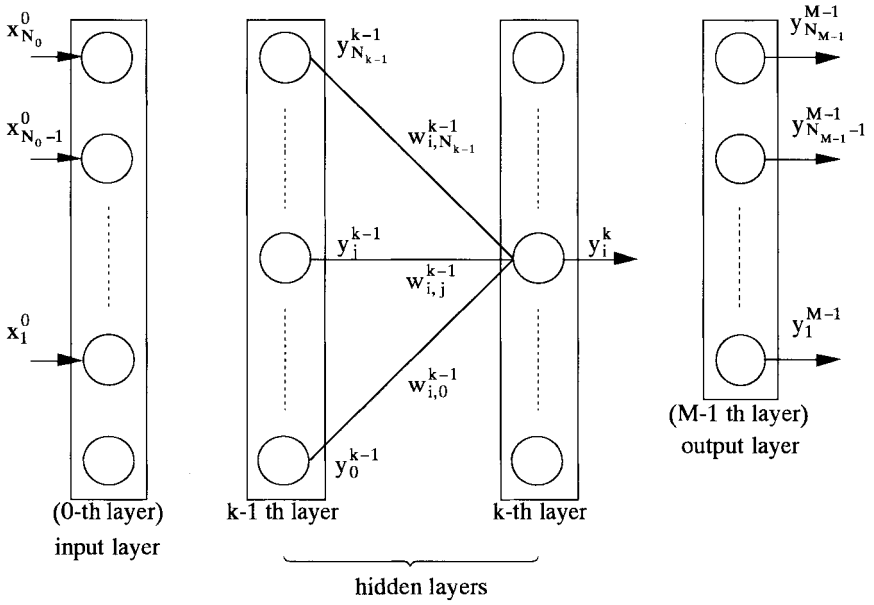

Fig. 1. Multilayered neural network.

the kth layer are given by

$$x_i^k = \sum_{j=0}^{N_{k-1}} w_{i,j}^{k-1} y_j^{k-1} \tag{1}$$

and

$$y_i^k = \frac{1}{1+\exp(-x_i^k)} \tag{2}$$

where $w_{i,j}$'s denotes the synaptic weighting factors which indicate the relative importance of each input h_j^{k-1} from the $(k-1)$th layer. The adaptability of this neural network is evaluated by using the discrepancy E (3) between the network outputs y_i^{M-1} $(i = 1, \cdots, N_{M-1})$ and the learning patterns d_i $(i = 1, \cdots, N_{M-1})$:

$$E = \tfrac{1}{2} \sum_{i=1}^{N_{M-1}} (y_i^{M-1} - d_i)^2. \tag{3}$$

The weighting factors are iteratively determined by a back-propagation algorithm. The correction terms in the iterations are given by the following equation:

$$\delta w_{i,j}^{k-1}(l) = \eta \frac{\partial E}{\partial w_{i,j}^{k-1}} + \alpha \delta w_{i,j}^{k-1}(l-1) \tag{4}$$

where l denotes the loop counter, and the parameters η and α are the learning rate and momentum factor, respectively.

III. Neural Network for Bias-Dependent HEMT's

We characterized the bias-dependent behavior of the HEMT in terms of the intrinsic elements of a conventional small-signal equivalent circuit.

The intrinsic element data depending on $V_{\rm gs}$ and $V_{\rm ds}$ are obtained from the S-parameters measurements performed at various bias settings [5].

We then defined a set of input data vectors $\boldsymbol{x}$ and teaching data vectors $\boldsymbol{d}$ for the neural network as

$$\boldsymbol{x} = (x_{1,l}^0, x_{2,l}^0) = \{s(V_{gs_l}), s(V_{ds_l})\} \tag{4}$$

$$\begin{aligned}\boldsymbol{d} &= (d_{1,l}, d_{2,l}, \cdots, d_{7,l}) \\ &= \{s[C_{\rm gs}(V_{gs_l}, V_{ds_l})], s[R_i(V_{gs_l}, V_{ds_l})], \\ &\quad \cdots, s[C_{\rm ds}(V_{gs_l}, V_{ds_l})]\}\end{aligned} \tag{5}$$

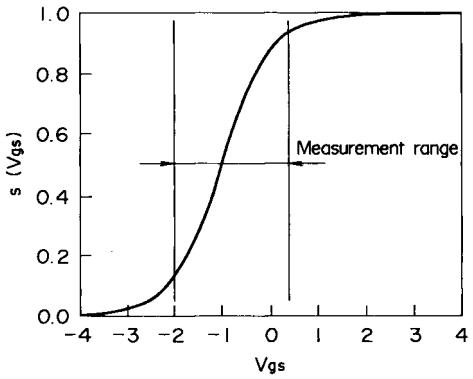

Fig. 2. Scaling function.

where subscript l $(l = 0, \cdots, L-1)$ denotes the number of data points, and s denotes the sigmoid function which scales the raw data into a convenient range for calculation. For example, the dominant range of $V_{\rm gs}$ is always between $(-V_p/5)$ and V_p, and outside this range, each element value tends to be saturated against $V_{\rm gs}$. Thus we defined s $(V_{\rm gs})$ significantly varied with $V_{\rm gs}$ in the range of interest (see Fig. 2). It was gradually saturated outside the particular measurement range. If the bias voltage exceeded the measurement range during simulation, the scaling function was supposed to keep the element value in the vicinity of the rational value. Thus, it is useful for calculation convergence as well as extrapolation.

If we use an individual network to characterize the intrinsic elements individually, each network structure is simplified. For example, a description of $C_{\rm gs}$ requires a three-layered network consisting of two neurons for the first layer, five for the second layer, and one for the third layer. Although the neural network can fit any type of data with a unique network, we desire the simplest structure possible. Through experiments, we found that a five-layered configuration composed of only 28 neurons adequately represents the seven large-signal parameters simultaneously. Fig. 3 shows our neural network model of an HEMT. We trained this neural network by using a batch-mode back-propagation algorithm [6] for several similar devices. In batch-mode back propagation, the network adaptability is

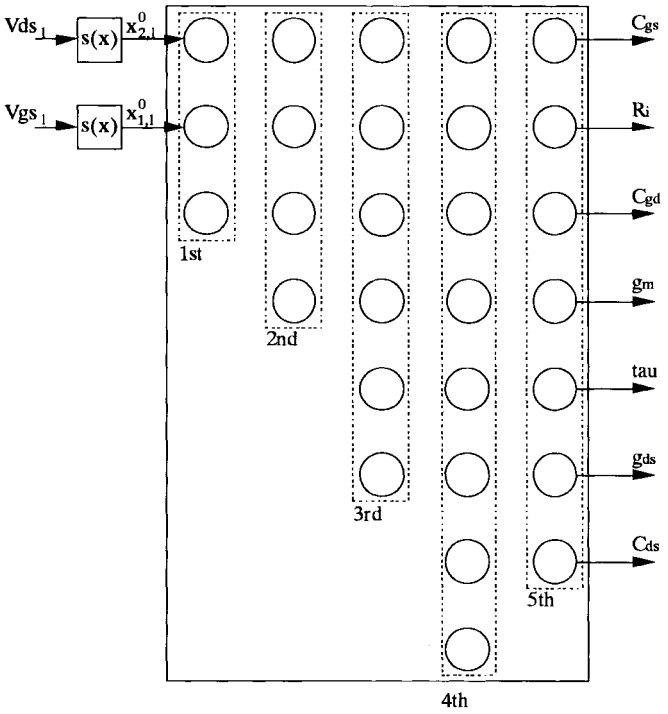

Fig. 3. Five-layered neural network. The areas enclosed by dashed lines are layers, and the circles are neurons. Input data $V_{\rm gs}$ and $V_{\rm ds}$ are scaled by a sigmoid function $s(x)$. The neuron at the bottom of each layer (except the output) provides the threshold values. The output layer generates bias-dependent intrinsic elements for particular bias voltages. Synaptic connections have been omitted in this figure.

evaluated by the following equation:

$$E = \frac{1}{2}\sum_{l=0}^{L-1}\sum_{i=1}^{N_{M-1}}\left(y_{i,l}^{M-1} - d_{i,l}\right)^2 = \sum_{l=0}^{L-1} E_l \tag{6}$$

where L denotes the number of bias points. The principal correction term in the iterations (3) is given by the following equation:

$$\frac{\partial E}{\partial w_{i,j}^{k-1}} = \sum_{l=0}^{L-1}\frac{\partial E_l}{\partial w_{i,j}^{k-1}}. \tag{7}$$

That is, the correction values are accumulated for all combinations of data points, making batch-mode back propagation effective for finding the optimum convergence for all combinations of data. We used a learning rate η of 0.8, and a momentum factor α of 0.9 for the training.

IV. Measurement

Using the neural network obtained in the Section IV, we characterized the intrinsic elements of an HEMT with a 0.25-μm-long and 100-μm-wide gate. Fig. 4 shows the fitting results for $C_{\rm gs}$. The marks denote actual data, and the solid lines are values calculated using the neural network. The rms error under 4% between the measured and calculated values can be achieved for individual elements.

In addition, we calculated the element values of this HEMT with several bias points. These were excluded from the fitting calculations. Fig. 4 also compares the calculated $C_{\rm gs}$ values to the actual data subsequently obtained. In this figure, the marks at $V_{\rm gs} = 0.4$ V ($V_{\rm ds} = 0.0$ to 3.0 V), and $V_{\rm ds} = 3.0$ V ($V_{\rm gs} = -0.8$ to 0.4 V) denote data measured afterwards, and the dashed lines denote values predicted by the neural network. Fig. 5 shows the same in the case of g_m.

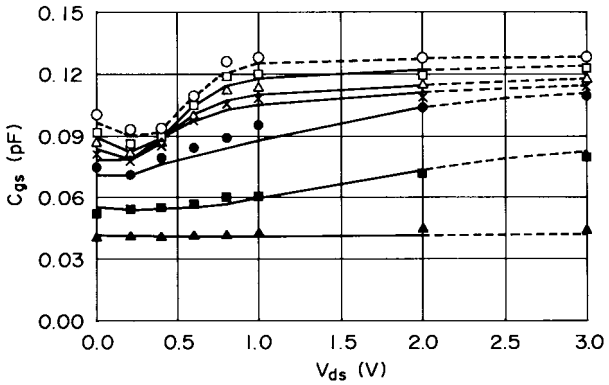

Fig. 4. Fitting and predicted results of $C_{\rm gs}$. The marks are measurements, and the solid-lines are the fitting results. The predictions were performed for $V_{\rm gs} = 0.4$ V and $V_{\rm ds} = 3.0$ V (dashed lines), and the measurements for these bias settings were obtained after the prediction. ○: $V_{\rm gs} = 0.4$ V, □: $V_{\rm gs} = 0.2$ V, △: $V_{\rm gs} = 0.0$ V, ×: $V_{\rm gs} = -0.2$ V, •: $V_{\rm gs} = -0.4$ V, ■: $V_{\rm gs} = -0.6$ V, △: $V_{\rm gs} = -0.8$ V.

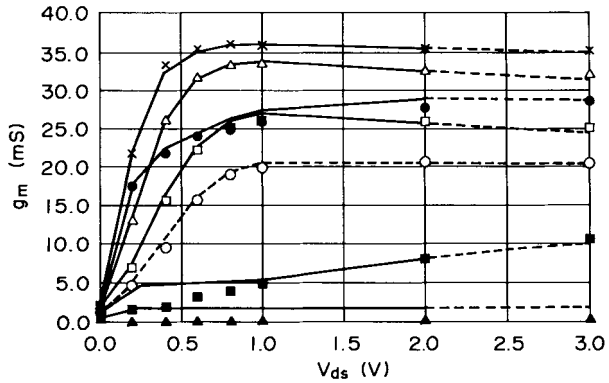

Fig. 5. Fitting and predicted results of g_m. The marks are measurements, and the solid lines are the fitting results. The predictions were performed for $V_{\rm gs} = 0.4$ V and $V_{\rm ds} = 3.0$ V (dashed lines), and the measurements for these bias settings were obtained after the prediction. ○: $V_{\rm gs} = 0.4$ V, □: $V_{\rm gs} = 0.2$ V, △: $V_{\rm gs} = 0.0$ V, ×: $V_{\rm gs} = -0.2$ V, •: $V_{\rm gs} = -0.4$ V, ■: $V_{\rm gs} = -0.6$ V, △: $V_{\rm gs} = -0.8$ V.

A well-trained neural network can generate stable and valid element values even for a bias which exceeds the measurement range.

V. Conclusions

We have reported an approach to describe the large-signal behavior of an HEMT by using a multilayered neural network. For future implementation on commercially available simulators, we represented the bias-dependent behavior of the HEMT in terms of conventional small-signal equivalent-circuit elements.

We found that a five-layered configuration composed of only 28 neurons will represent seven bias-dependent intrinsic elements from $V_{\rm gs}$ and $V_{\rm ds}$ simultaneously. We adopted this neural network with the batch-mode back-propagation algorithm and obtained close agreement with the actual data. Furthermore, we calculated element values at several bias points outside the measurement range and obtained a good extrapolation.

The multilayered neural network can describe all of the large-signal elements with a configuration simpler than any previously reported.

References

[1] H. Staz, P. Newman, I. Smith, R. Pucel, and H. Haus, "GaAs FET device and circuit simulation in SPICE," *IEEE Trans. Electron Devices*, vol. ED-34, pp. 160–169, Feb. 1987.

[2] J. W. Bandler, R. M. Biernacki, S. H. Chen, J. Song, S. Ye, and Q. Zhang, "Analytical unified dc/small-signal/large-signal circuit design," *IEEE Trans. Microwave Theory Tech.*, vol. 39, pp. 1076–1082, July 1991.
[3] D. E. Root, S. Fan, and J. Meyer, "Technology independent large signal non quasi-static FET models by direct construction from automatically characterized device data," in *Proc. 21st European Microwave Conf.*, Stuttgart, Germany, Sept. 1991, pp. 927–923.
[4] A. H. Zaabab, Q. Zhang, and M. Nakhla, "A neural network modeling approach to circuit optimization and statistical design," *IEEE Trans. Microwave Theory Tech.*, vol. 43, pp. 1349–1358, Jun. 1995.
[5] K. Shirakawa, H. Oikawa, T. Shimura, Y. Kawasaki, Y. Ohashi, T. Saito, and Y. Daido, "An approach to determining an equivalent circuit of HEMT's," *IEEE Trans. Microwave Theory Tech.*, vol. 43, pp. 499–503, Mar. 1995.
[6] J. A Hertz, A. Krogh, and R. B. Palmer, *Introduction to the Theory of Neural Computation.* Reading, MA: Addison-Wesley, 1991, pp. 141–159.

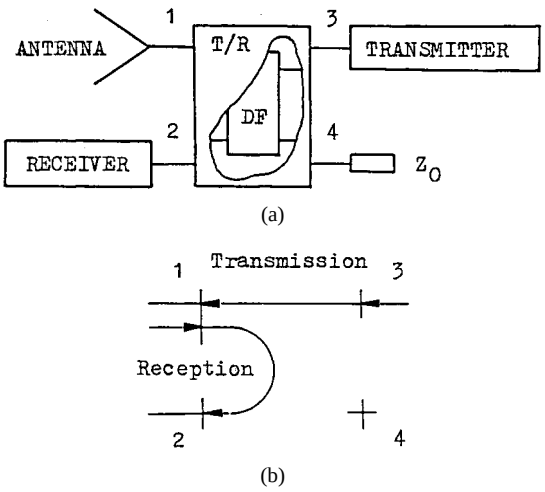

Fig. 1. A transmit/receive module. (a) Functional block diagram. (b) Signal flow chart

Novel Microstrip-Line Directional Filters

Stanislaw Rosloniec and Tahar Habib

***Abstract*— This paper presents two new structures of four-port microwave directional filters incorporating microstrip-line resonators, uniplanar 180° phase-reversal units, and two or four identical p-i-n diodes. These filters provide substantially improved frequency characteristics compared to the conventional constructions. The unique feature of them is that they ensure high-level isolation independent of frequency between opposite ports. Due to this electrical property the proposed filters may be suitable for some pulse-radar applications.**

***Index Terms*—Microstrip-line directional filters, microwave filters, T/R modules.**

I. Introduction

Directional filters are indispensable components of transmit/receive (T/R) modules (see Fig. 1) used in various communication systems. The conventional nonadjustable structures of them are comprehensively described in the literature [1]–[3]. These filters, however, cannot be applied directly in systems with transmit and receive signals of the same or very close frequencies. Furthermore, they do not ensure perfect isolation independent of frequency between opposite ports marked as 2 and 3 in Fig. 1. Consequently, the receiver cannot be sufficiently protected from the transmitter over the required frequency range. In order to eliminate the above disadvantages two electronically switchable microstrip-line directional filters have been developed. The construction and electrical performance of these filters are the subject of this paper. The validity of the presented theoretical results has been confirmed experimentally for the frequency range of 0.5–1.5 GHz.

Manuscript received February 21, 1996; revised May 19, 1997.

The authors are with the Institute of Radioelectronics, Warsaw University of Technology, 00-665 Warsaw, Poland.

Publisher Item Identifier S 0018-9480(97)06075-4.

II. Microwave Directional Filters with Two and Four p-i-n Diodes

The microstrip line configurations of the filters being investigated are shown in Fig. 2. These filters are composed of two microstrip-line resonators, two or four p-i-n diodes, and a 180° phase-reversal unit which is placed at the center of one resonator. Near this center the standing wave forms a short-circuit node. Therefore, the equivalent inductances L of this unit [Fig. 3(a) and (b)], have to be especially small. This requirement explains why in the proposed filters relatively wide and short copper strips are used as electrical bonds. A constructional view of the proposed design, using the slotline hollow patches for broad-band open conditions, is illustrated in Fig. 3(c) and (d) [4], [5]. The second resonator including the 180° phase-reversal unit should be electrically uniform over the entire length, so that at any cross section its characteristic impedance will be the same. Thus, the finite ground plane of the microstrip line caused by the slotline hollow patches has to be taken into account in the design process.

The first filter (DF-2) presented in Fig. 2(a) is asymmetric with respect to the horizontal x–x' and vertical y–y' planes, and for this reason cannot be analyzed by using the even- and odd-mode excitation method [3], [6]. Consequently, the following numerical algorithm is proposed here for this purpose. The idea of this algorithm is similar to that used in [7]. For any pair of ports, k and l, the filter DF-2 may be treated as a reciprocal two-port network incorporating two partial two-ports P_{kl} and Q_{kl} connected in parallel, as shown in Fig. 4(a). For clarification of further considerations let us assume that the scattering parameters S_{11}, S_{14}, S_{41}, and S_{44} of the filter are evaluated. In this case, two-ports P_{14} and Q_{14} are similar to those shown in Fig. 4(b) and (c). The transfer matrices $(ABCD)_P$ and $(ABCD)_Q$ of these circuits can be easily calculated by multiplying the corresponding matrices $(ABCD)$ of the elementary cascade components [8]. When the resulting matrices $(ABCD)_P$ and $(ABCD)_Q$ are known, then we can evaluate the admittance matrices $[Y]_P$ and $[Y]_Q$ related to them. The total admittance matrix $[Y] = [Y]_P + [Y]_Q$ makes it possible to calculate the scattering parameters S being sought. For this purpose we can use the well-known matrix transformations $[Y] \rightarrow [S]$, [8], [9]. The